Polymers **2014**, *6*, 613-633; doi:10.3390/polym6030613

OPEN ACCESS

polymers

ISSN 2073-4360

www.mdpi.com/journal/polymers

Article

RC Beams Strengthened with Mechanically Fastened Composites: Experimental Results and Numerical Modeling

Enzo Martinelli, Annalisa Napoli, Bruno Nunziata and Roberto Realfonzo *

Department of Civil Engineering, University of Salerno, Via Giovanni Paolo II 132, Fisciano (SA) 84084, Italy; E-Mails: e.martinelli@unisa.it (E.M.); annapoli@unisa.it (A.N.); bnunziata@unisa.it (B.N.)

* Author to whom correspondence should be addressed; E-Mail: rrealfonzo@unisa.it; Tel.: +39-089-964085; Fax: +39-089-968739.

Received: 18 December 2013; in revised form: 17 February 2014 / Accepted: 19 February 2014 / Published: 5 March 2014

Abstract: The use of mechanically-fastened fiber-reinforced polymer (MF-FRP) systems has recently emerged as a competitive solution for the flexural strengthening of reinforced concrete (RC) beams and slabs. An overview of the experimental research has proven the effectiveness and the potentiality of the MF-FRP technique which is particularly suitable for emergency repairs or when the speed of installation and immediacy of use are imperative. A finite-element (FE) model has been recently developed by the authors with the aim to simulate the behavior of RC beams strengthened in bending by MF-FRP laminates; such a model has also been validated by using a wide experimental database collected from the literature. By following the previous study, the FE model and the assembled database are considered herein with the aim of better exploring the influence of some specific aspects on the structural response of MF-FRP strengthened members, such as the bearing stress-slip relationship assumed for the FRP-concrete interface, the stress-strain law considered for reinforcing steel rebars and the cracking process in RC members resulting in the well-known tension stiffening effect. The considerations drawn from this study will be useful to researchers for the calibration of criteria and design rules for strengthening RC beams through MF-FRP laminates.

Keywords: FRP composites; external strengthening; structural rehabilitation

---

1. Introduction

The use of mechanically-fastened (MF) fiber-reinforced polymer (FRP) systems has recently emerged as an effective solution for the flexural strengthening of reinforced concrete (RC) beams. The technique consists of pre-cured FRP laminates with enhanced bearing strength, which can be fastened to the external surface of concrete members through a variety of steel anchors, *i.e.*, nails or powder actuated fasteners ("PAF"), anchor bolts, concrete screws or a combination thereof. Unlike the externally-bonded (EB) FRP method, the MF-FRP system is particularly fit for emergency repairs, where the ease of installation and reversibility are primary requirements; also, it is less vulnerable to fail prematurely by FRP delamination, which abruptly reduces the flexural strength gain and affects the beam ductility.

Figure 1a shows the laminates currently available in the market; they are glass- and carbon-vinyl ester pultruded strips with enhanced transverse and bearing strength by means of embedded fiberglass mats [1]. The width and thickness of the laminates are 102 and 3.2 mm, respectively. They may be pre-drilled with holes at the required fastener spacing to receive fasteners, but they can be easily field drilled or cut into shorter lengths using standard carpenter tools.

Figure 1b depicts the types of anchors used to secure the laminate to concrete. The PAF system consists of pins embedded into base materials by means of a gunpowder charge; the installation requires times shorter than for concrete screw/wedge bolts and wedge anchors. Pre-drilling holes in the concrete is strongly recommended in order to reduce detrimental cracking phenomena. The use of the PAF system is particularly suitable when the compression strength of the concrete is less than 27 MPa. The presence of hard aggregates can prevent the fasteners from fully penetrating the concrete substrate [2].

Figure 1. Components of the mechanically-fastened fiber-reinforced polymer (MF-FRP) system: (**a**) FRP strip; (**b**) fasteners.

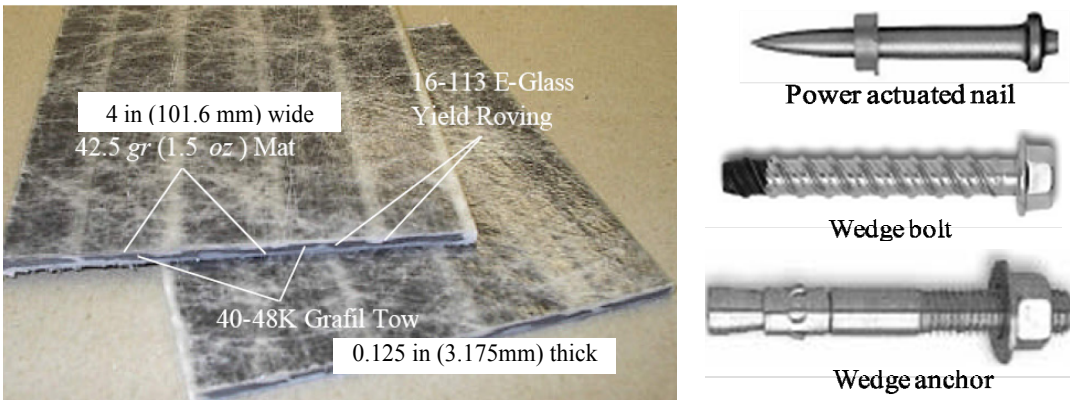

(**a**) (**b**)

Wedge bolts are single-piece, heavy duty anchors that are driven into pre-drilled holes. Driving of the wedge bolt can be performed with a common rotary drill or impact wrench. As for the PAFs, the efficiency of wedge bolts is dependent on the presence of hard aggregates. Preliminary studies [3] indicate that this use is not recommended for concrete with a compression strength greater than 27 MPa and with hard aggregates in the mix design.

In spite of longer installation times, wedge anchors can be used for any type of concrete; they are driven through the laminate into predrilled holes until the nut and washer are firmly secured against the laminate. The anchors are typically tightened by turning the nut with an electrical drill with torque control, according to the specifications of fastener manufactures.

A recently published state-of-the-art review of the experimental research has provided compelling evidence of the effectiveness and viability of using MF-FRP laminates to rehabilitate RC beams and slabs [4]. It has shown that with an appropriate fastener layout and FRP laminate properties, the strength increases are comparable to those of EB-FRP-strengthened members, but with greater displacements exhibited at collapse. Furthermore, experimental tests have proven that the mechanically-fastened composite system is an effective technique for improving the flexural capacity of corrosion-damaged RC beams [5]. Finally, applications of the MF-FRP technique to wood and timber structural members have been reported [6,7].

Several analytical and numerical studies have been carried out throughout-years with the aim of predicting the behavior of RC members strengthened in bending with MF-FRP systems: a state-of-the-art review on this topic has been recently published by Napoli *et al.* [8]. As highlighted therein, the first analytical models were based, for the sake of simplicity, on the hypothesis of the "conservation of plane sections" between the concrete and the FRP, as generally accepted for EB-FRP-strengthened members. Despite their ease of application, such models have often provided inaccurate predictions which were primarily attributed to ignoring the slip between the concrete and FRP strip. Therefore, novel proposals accounting for the concrete-FRP interfacial behavior were recently formulated by Lee *et al.* [9] and Nardone *et al.* [10]. In particular, Lee *et al.* [9] experimentally calibrated a reduction factor for the FRP strain estimated by assuming a perfect bond (no slip). Nardone *et al.* [10], instead, modeled the slip by means of a linear function of the position along the longitudinal axis of the FRP laminate, with a maximum value at the first fastener and zero slip at midspan for the case of symmetric loads.

Finite-element (FE) models were also developed to simulate the behavior of MF-FRP-strengthened RC beams and slabs. To this aim, the first work Napoli *et al.* [11] formulated a FE procedure in which a continuous connection was assumed throughout the interface between the FRP laminate and RC beam, in spite of the discrete nature of mechanical anchors. Although this assumption led to results as accurate as in the case of EB-FRP systems, it introduced a certain level of approximation, especially in the case of either coarse or unequally-spaced fasteners. Thus, the authors have recently developed a novel FE model which is based on the explicit assumption of discrete connection between concrete and FRP. Such a model, already detailed and validated in Martinelli *et al.* [12], is used in this study to simulate experimental tests available in the literature and relative to MF-FRP-strengthened RC beams and one-way slabs; most of these tests are included in a more general database published by Brown *et al.* [4].

The numerical simulations discussed herein were mainly aimed at investigating the influence of some specific aspects on the structural response of MF-FRP-strengthened members, such as the bearing stress-slip relationship assumed for the FRP-concrete interface, the stress-strain law considered for reinforcing steel rebars and the cracking process in RC members, which is often disregarded in modeling methods. The considerations drawn from this study will be useful to researchers for the calibration of criteria and design rules for the strengthening RC beams through MF-FRP laminates.

2. Outline of the Proposed 1D-FE Model

This section presents the key features of the novel 1D finite-element model formulated for simulating the flexural behavior of RC beams strengthened by MF-FRP. Such a model, deeply described in [12], is based on a discrete connection between the RC beam and the FRP strip, and can be potentially used for analyzing other similar modeling problems, such as those related to the external reinforcement of masonry or wood members.

2.1. Assumptions and Formulation of the Finite Element

The proposed finite element is obtained by assembling the following three components (see Figure 2):

- a 1D element that represents the behavior of Euler–Bernoulli's RC beam;
- a rod element that simulates the mechanical behavior of an FRP laminate;
- two springs that simulate the behavior of the fasteners and are only translational in the direction of the beam axis.

Figure 2. Key components of the proposed 1D finite-element.

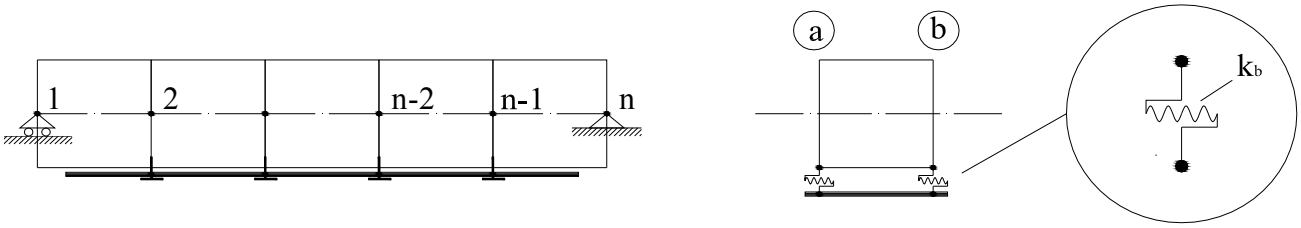

The relevant displacement and force components of the finite element "*e*", whose nodes are labelled as "*a*" and "*b*" are collected in the two following vectors $u^{(e)}$ and $f^{(e)}$, respectively, and represented in Figure 3:

$$u^{(e)} = \begin{Bmatrix} u_{f,a} \\ u_a \\ \varphi_a \\ v_a \\ u_{f,b} \\ u_b \\ \varphi_b \\ v_b \end{Bmatrix} \quad f^{(e)} = \begin{Bmatrix} N_{f,a} \\ N_a \\ M_a \\ V_a \\ N_{f,b} \\ N_b \\ M_b \\ V_b \end{Bmatrix} \tag{1}$$

By introducing the stiffness matrix, $k^{(e)}$, of the finite element "*e*" and the vector of equivalent nodal forces, $f_0^{(e)}$, the following matrix relationship between vectors $u^{(e)}$ and $f^{(e)}$ can be written:

$$f^{(e)} = k^{(e)} u^{(e)} + f_0^{(e)} \tag{2}$$

The matrix, $k^{(e)}$, and the vector $f_0^{(e)}$, can be both determined by taking into account the contributions corresponding to the three abovementioned components (beam, rod and springs). Details about the model formulation are omitted herein for the sake of brevity and can be found in [12].

Figure 3. Force and displacement components for the proposed finite element.

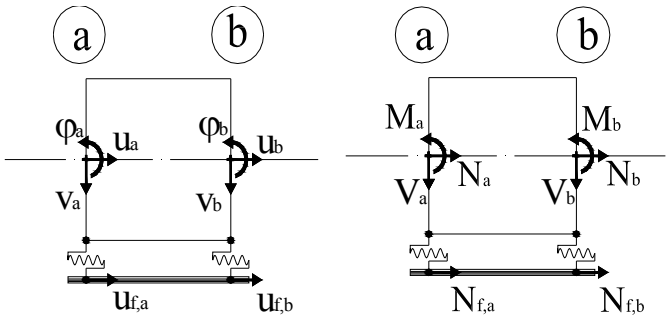

2.2. Nonlinear Analysis Procedure

RC beams with MF-FRP plates can be discretized through the *n* aforementioned finite elements, and the following relevant assumptions have been implicitly considered:

- the flexural stiffness of the FRP laminate is neglected, and only the axial one is considered;
- equal vertical displacements occur in the connected RC slab and FRP laminate elements;
- shear deformations of the RC slab are neglected.

The generic finite element is then used for nonlinear analyses through a fiber discretization of the beam cross-section and by implementing an iterative convergence procedure based on the "tangent" value approach to account for material nonlinearity, including concrete, steel and the concrete–FRP interface, as already demonstrated for the case of EB-FRP-strengthened RC members [13].

Figures 4 and 5 depict the generalized stress-strain laws considered in the numerical analyses to simulate the behavior of concrete in compression [14] and tension [15] and of steel rebars, respectively, whereas the FRP strip was simulated through an elastic-brittle behavior.

Figure 4. Stress-strain law for concrete.

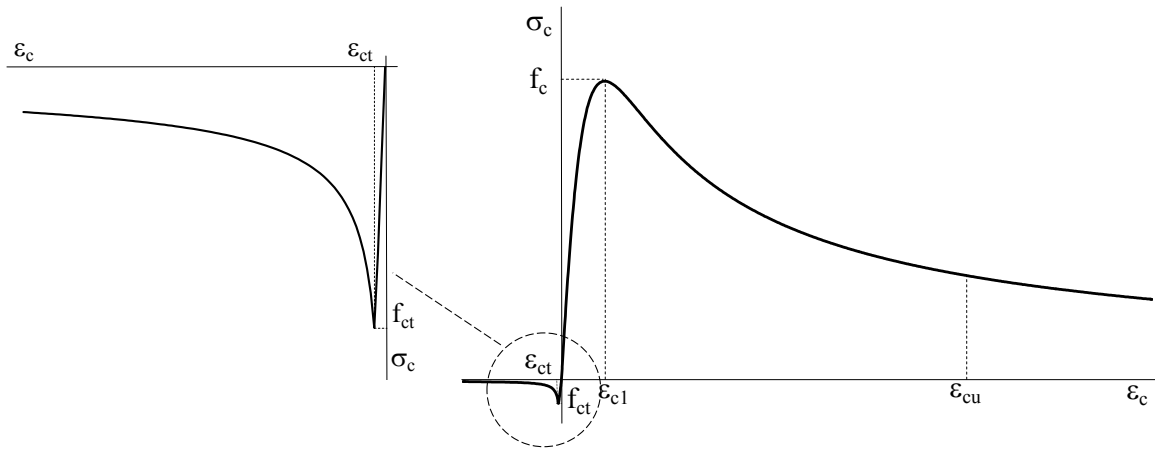

Figure 5. Alternative stress-strain laws for steel reinforcing bars: "accurate" (**a**) and "simplified" (**b**) bilinear models.

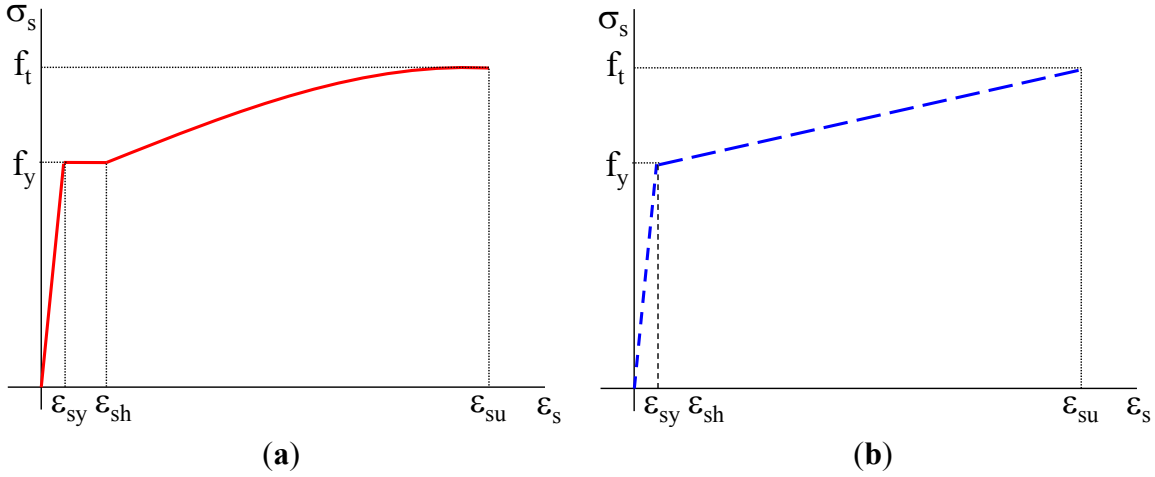

As shown in Figure 5, two stress-strain (σ_s-ε_s) relationships have been taken into account for simulating the behavior of steel rebars. The first one (Figure 5a) is characterized by an initial elastic behavior, a yielding phenomenon with constant stress and, then, by a hardening response; particularly, a parabolic branch was considered after the yielding plateau, which was assumed to develop up to the hardening strain, ε_{su}. The elastic-plastic σ_s-ε_s law of Figure 5b, instead, is of a bilinear type and represents a possible simplification of the more accurate relationship shown in Figure 5a. It is highlighted that in the numerical analyses, the values of ε_{sh}, ε_{su} and ultimate strength (f_t) were always assumed equal to 0.003, 0.07 and 1.20 f_y, respectively, where f_y is the yield strength of longitudinal steel rebars. More details about the considered stress-strain laws can be found in [12].

Figure 6, instead, shows the bearing stress-interface slip (σ_f-s) relationships employed to simulate the response of the connecting devices, *i.e.*, of shot or screwed fasteners. In particular, the trilinear laws selected in the case of screws with (w/) and without (w/o) washers (Models 2b and 3 in Figure 6) are those proposed by the authors in a previous study [16]; the other ones, used in the case of shot or screwed fasteners w/ washer (Models 1 and 2a in Figure 6), are those found by Elsayed *et al.* [17].

Figure 6. Bearing stress-slip relationship describing the FRP strip-concrete interaction.

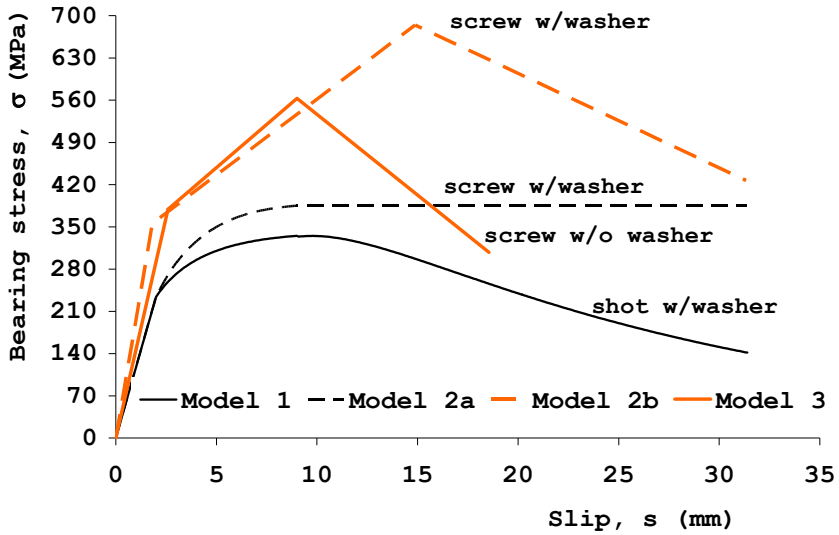

It is highlighted that although three of the four σ_f-s laws exhibit a softening branch, the actual values of the interfacial slip observed in the modeling of the MF-FRP-strengthened beams never fall in such a branch; therefore, modeling issues related to strain localization can be overcome.

A nonlinear solution procedure can be implemented to determine the response of the structural system under self-weight and other external loads. First of all, the distributed loads corresponding to the beam self-weight are applied in force control, and then, the procedure works in the displacement control for simulating the effect of the imposed external loads. The analysis foresees several steps of imposed displacement increments and, in each step, an iterative search of the forces corresponding to the imposed displacement. In particular, at the i-th analysis step, the j-th iteration firstly provides an "elastic prediction" of the solution, based on the tangent stiffness matrix $K_{T,i}^{(j-1)}$, at the end of the previous iteration:

$$\Delta U_{el,i}^{(j)} = \left[K_{T,i}^{(j-1)} \right]^{-1} \Delta\lambda_{el,i}^{(j)} F_q \tag{3}$$

where $\Delta\lambda_{el,i}^{(j)}$ is the current value of the elastic incremental force multiplier, F_q is a global vector describing the "shape" of the external load applied to the beam and $\Delta U_{el,i}^{(j)}$ is the vector of the elastically predicted displacement increments (at the j-th iteration of the i-th load step).

Equation (3) can be solved through classical numerical procedures of the finite element modeling (FEM) based on imposing that one of the $\Delta U_{el,i}^{(j)}$ components (*i.e.*, the mid-span deflection) is equal to the controlled displacement increment $\Delta w_i^{(j)}$.

For each element, the local displacement increment $\Delta u_{el,i}^{(j)}$, can be obtained through $\Delta U_{el,i}^{(j)}$, and then, the elastic prediction of the j-th iteration can be completed by determining both the local stress increment $\Delta\sigma_{el,i}^{(j)}$, and the corresponding local strain vector, $\varepsilon_{el,i}^{(j)}$.

Then, the "plastic correction" can be performed by evaluating the stress increments, $\Delta\sigma_{pl,i}^{(j)}$, actually corresponding to the current strain increments, $\varepsilon_{el,i}^{(j)} - \varepsilon_{el,i-1}$, where the latter is the strain vector at convergence of the $(i - 1)$-th analysis step. The "plastic correction" ends as the nonlinear stress increment, $\Delta\sigma_{pl,i}^{(j)}$, is determined and the corresponding stiffness matrix is updated by considering the actual nonlinear response of the three components mentioned in Subsection 2.1.

At the end of this sub-step and after having assembled the new local stiffness matrices, $k_{T,i}^{(j)}$, the global tangent matrix, $K_{T,i}^{(j)}$, and the corresponding external force increment, $\Delta F_{pl,i}^{(j)}$, can be obtained:

$$\Delta F_{pl,i}^{(j)} = K_{T,i}^{(j)} \Delta U_{el,i}^{(j)} \tag{4}$$

Then, the $(j + 1)$-th iteration can be carried out for determining the force and displacement increment according to a relationship similar to Equation (3). The iteration procedure proceeds for the current analysis step, until two following iterations yield displacement increments, whose difference is the smaller of a given tolerance δ:

$$\left| \Delta U_{el,i}^{(j+1)} - \Delta U_{el,i}^{(j)} \right| < \delta \tag{5}$$

At the end of the i-th analysis step, the failure conditions of both materials (possibly achieving the ultimate strain) and fasteners (possibly attaining the ultimate slip value) should be checked. If either of such materials or one of the fasteners achieves such a conventional failure condition, the analysis finishes; otherwise the analysis proceeds with the $(i + 1)$-th step, as described above.

3. The Database

A wide database was assembled from the literature, which collects a total of 93 four point-bending tests performed on RC beams/slabs externally strengthened with MF-FRP laminates. Figure 7 shows a schematic of the tests under consideration. It is highlighted that the considered database represents a further updating of that which was recently published in [12].

Figure 7. The configuration of four point-bending tests collected from the literature.

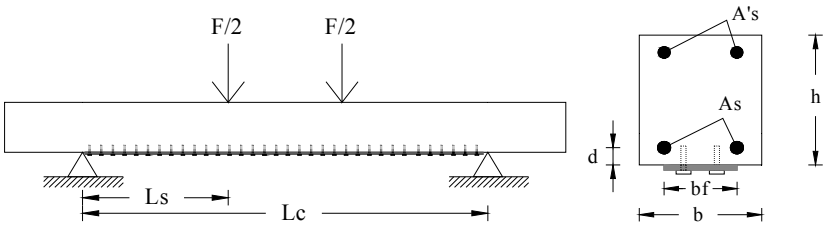

Table 1 summarizes the relevant geometrical and mechanical properties of the test specimens and the experimental load values measured at yielding and peak conditions. Table 2, instead, provides information about the MF-FRP strengthening layouts.

In addition to the symbols clarified in Figure 7, the other labels included in Tables 1 and 2 are reported in the following:

- f_c = average value of concrete cylinder compressive strength;
- f_y = average value of yield strength of longitudinal steel reinforcement, when obtained by tensile tests (alternatively, information about the steel grade is provided);
- F_y = experimental value of the force measured at the beam yielding during the test;
- F_{max} = experimental value of the peak force measured during the test;
- L_f, E_f, f_f = length, elastic modulus and tensile strength of the employed FRP strip, respectively;
- d_a, L_a = diameter and shank length of the employed fasteners (shot, screw or wedge), respectively, which were provided or not with steel washer.

The fasteners were arranged on single or multiple rows (N = 1, 2, 4) according to aligned ("-a") or staggered ("-s") configurations or combinations thereof ("a-s").

As observed from the tables, test specimens have different sizes of cross-section, with values of the height-to-width (h/b) ratios spanning from 0.5 ("slab-type") to 1.67 ("beam"-type"); the clear lengths range from 1067 mm (small-scale members) to 3505 mm (large-scale members).

Table 1. The geometry and mechanical properties of considered test specimens and main results.

Source	Test	L_c (mm)	L_s (mm)	$b \times h$ (mm^2)	A'_s (mm^2)	A_s (mm^2)	d (mm)	f_c (MPa)	Steel type f_y (MPa)	F_y [1] KN	F_{max} [1] KN
	U-W-2	3505	1372							*186*	*210*
	U-W-4	2134	686							377	*427*
	U-W-5	2642	940							268	*344*
Borowicz (2002) [18]	U-W-6	3353	1295	305 × 305	143	1013	51	44.7	Grade 60	*193*	*243*
	U-W-7	3454	1346							*185*	*234*
	U-W-8	3505	1372							*182*	*233*
	U-W-9	3505	1372							*202*	*257*

Table 1. *Cont.*

Source	Test	L_c (mm)	L_s (mm)	$b \times h$ (mm^2)	A'_s (mm^2)	A_s (mm^2)	d (mm)	f_c (MPa)	Steel type f_y (MPa)	F_y [1] KN	F_{max} [1] KN
Ebead (2011) [19]	M-F-D10-1	2250	850	150 × 250	101	157	25	41	540	51	*70*
	M-F-D10-2					157	25	38	540	70	*77*
	M-F-D12-1					226	26	38	550	79	*99*
	M-F-D12-2					226	26	39	550	75	*105*
	M-F-D16-1					402	28	40	530	106	*130*
	M-F-D16-2					402	28	39	530	110	*132*
	M-P-D10-1					157	25	37	540	44	*55*
	M-P-D10-2					157	25	38	540	39	*60*
	M-P-D12-1					226	26	36	550	68	*79*
	M-P-D12-2					226	26	39	550	68	*81*
	M-P-D16-1					402	28	36	530	101	*105*
	M-P-D16-2					402	28	41	530	-	*110*
Ekenel *et al.* (2005) [20]	S-4-F	1829	304	254 × 165	143	214	45	27.6	414	57	*72*
El-Maaddawy (2013) [5]	C0-PAF-32	2800	1200	250 × 275	339	100	34	30.5	500	*85*	*122*
	C0-PAF-52									*85*	*134*
	C0-EAB									*90*	*132*
	C0-TAB									*90*	*135*
	C1-PAF-32									*80*	*95*
	C1-PAF-52									*80*	*109*
	C1-EAB									*85*	*125*
	C1-TAB									*85*	*129*
	C2-PAF-32									*75*	*84*
	C2-PAF-52									*75*	*87*
	C2-EAB									*75*	*110*
	C2-TAB									*75*	*128*
El-Maaddawy *et al.* (2013) [21]	C0-F50-32	1250	550	150 × 210	226	100	30	32	538	*80*	*86*
	C0-F100-32									*85*	*87*
	C0-F100-32-2									*85*	*88*
	C0-F50-52									*85*	*94*
	C0-F100-52									*85*	*90*
	C1-F50-32									*80*	*90*
	C1-F100-32									*80*	*87*
	C1-F100-32-2									*80*	*88*
	C1-F50-52									*80*	*90*
	C1-F100-52									*70*	*81*
	C2-F50-32									*70*	*80*
	C2-F100-32									*75*	*81*
	C2-F100-32-2									*80*	*84*
	C2-F50-52									*70*	*76*
	C2-F100-52									*70*	*78*
	C3-F50-52									*65*	*74*
	C3-F100-52									*70*	*83*
Galati *et al.* (2007) [22]	M-F-P-2	2200	600	200 × 250	226	226	29	31.5	462	87	*131*

Table 1. *Cont.*

Source	Test	L_c (mm)	L_s (mm)	$b \times h$ (mm^2)	A'_s (mm^2)	A_s (mm^2)	d (mm)	f_c (MPa)	Steel type f_y (MPa)	F_y [1] KN	F_{max} [1] KN
Lamanna (2002) [23]	D-1	1168	483					42		*52*	*61*
	D-2	1168	483					42		*52*	*58*
	E-1	1168	483					42		*51*	*55*
	E-2	1168	483					42		*51*	*61*
	J-1	1168	483					42		*50*	*54*
	L-1	1067	432					42		*55*	*56*
	T-1	1067	432					42		*56*	*62*
	T-2	1067	432					42		*59*	*67*
	T-3	1067	432					42		*54*	*61*
	F-1	1168	483	153 × 153	143	254	50	21	Grade 60	*48*	*52*
	G-1	1168	483					21		*49*	*50*
	K-1	1168	483					21		*47*	*50*
	M-1	1067	432					21		*53*	*55*
	N-1	1067	432					21		*57*	*57*
	P-1	1067	432					21		*60*	*62*
	Q-1	1067	432					21		*56*	*56*
	R-1	1067	432					21		*56*	*62*
	R-2	1067	432					21		*56*	*59*
	U-1	1067	432					21		*53*	*55*
Lamanna *et al.* (2001) [24]	F-42-S-102-1R	1067	432	153 × 153	143	254	39	42	Grade 60	*59*	*67*
	F-21-S-102-2R							21		*56*	*59*
Bank *et al.* (2002) Lamanna *et al.* (2004) [25,26]	S-4-Y-AL32	3353	1118	305 × 305	143	1013	51	35.3	Grade 60	*225*	*255*
	I-4-N-AL32									*233*	*253*
	I-4-Y-AL32									*239*	*269*
	I-4-Y-AL32-R									*234*	*279*
	I-8-Y-AL32									*248*	*273*
	H1.5-4-YAL32									*249*	*262*
	H1.5-4-Y-AL42D									*244*	*273*
	H1.5-4-Y-AL47D									*249*	*293*
	H1.5-4-Y-AL47D-3									*249*	*285*
	H1.5-4-Y-AL47D-3R									*249*	*283*
	H1.5-8-Y-AL32									*266*	*266*
	H1.0-4-Y-AL47D-5									*219*	*243*
Lee *et al.* (2007) [27]	1	1370	610	200 × 150	157	226	40	34.5	Grade 60	79	84
	2	1370	610	200 × 150	157	226	40	34.5	Grade 60	78	92
Martin and Lamanna (2008) [28]	6-L	3353	1219	305 × 305	143	1013	51	48	Grade 60	*185*	*203*
	6-S									*196*	*211*
	10-L									*182*	*206*
	12-L									*192*	*213*
Napoli *et al.* (2008) [11]	MF-1-L	3048	1219	305 × 152	-	380	25	26.7	Grade 60	42	*61*
	MF-1-S									41	*56*
	MF-2-L									36	*56*
	MF-2-S									35	*50*

Note: [1] The experimental values indicated in the published papers are reported in italics, whereas the remaining results have been approximately found by the authors.

Table 2. Details on the strengthening layouts. N-a, aligned; -s, staggered.

Source	Test	b_f (mm)	t_f (mm)	L_f (mm)	E_f (GPa)	f_f (MPa)	Fastener type	d_a (mm)	L_a (mm)	Washer	# rows
Borowicz (2002) [18]	U-W-2	102	3.2	3404	56.5	494	PAF	4.5	47	YES	2-a
	U-W-4			2134		494					2-a
	U-W-5			2642		494					2-a
	U-W-6			3251		743					2-a
	U-W-7			3048		743					2-a
	U-W-8			2997		743					2-a
	U-W-9		6.4	3404		743					2-a
Ebead (2011) [19]	M-F-D10-1	102	3.2	2200	72	1003	Screw	4.76	37	YES	2-a
	M-F-D10-2			2200							1-a/2-a
	M-F-D12-1			2200							2-a
	M-F-D12-2			2200							1-a/2-a
	M-F-D16-1			2200							2-a
	M-F-D16-2			2200							1-a/2-a
	M-P-D10-1			1350							2-a
	M-P-D10-2			1350							1-a/2-a
	M-P-D12-1			1350							2-a
	M-P-D12-2			1350							1-a/2-a
	M-P-D16-1			1350							2-a
	M-P-D16-2			1350							1-a/2-a
Ekenel *et al.* (2005) [20]	S-4-F	102	3.2	1778	62	531	Wedge anchor	9.5	40.3	YES	1-s
El-Maaddawy (2013) [5]	C0-PAF-32	102	3.2	2600	62	852	PAF	4	32	NO	2-a
	C0-PAF-52						PAF	4	52	NO	2-a
	C0-EAB						Wedge	8	55	YES	1-s
	C0-TAB						Screw	8	55	NO	1-s
	C1-PAF-32						PAF	4	32	NO	2-a
	C1-PAF-52						PAF	4	52	NO	2-a
	C1-EAB						Wedge	8	55	YES	1-s
	C1-TAB						Screw	8	55	NO	1-s
	C1-PAF-32						PAF	4	32	NO	2-a
	C1-PAF-52						PAF	4	52	NO	2-a
	C1-EAB						Wedge	8	55	YES	1-s
	C1-TAB						Screw	8	55	NO	1-s
El-Maaddawy *et al.* (2013) [21]	C0-F50-32	51	3.2	1050	62	852	PAF	4	32	NO	1-a
	C0-F100-32	102							32		1-a
	C0-F100-32-2	102							32		2-a
	C0-F50-52	51							52		1-a
	C0-F100-52	102							52		1-a
	C1-F50-32	51							32		1-a
	C1-F100-32	102							32		1-a
	C1-F100-32-2	102							32		2-a
	C1-F50-52	51							52		1-a
	C1-F100-52	102							52		1-a
	C2-F50-32	51							32		1-a
	C2-F100-32	102							32		1-a
	C2-F100-32-2	102							32		2-a
	C2-F50-52	51							52		1-a
	C2-F100-52	102							52		1-a
	C3-F50-52	51							52		1-a
	C3-F100-52	102							52		1-a

Table 2. *Cont.*

Source	Test	b_f (mm)	t_f (mm)	L_f (mm)	E_f (GPa)	f_f (MPa)	Fastener type	d_a (mm)	L_a (mm)	Washer	# rows
Galati *et al.* (2007) [22]	M-F-P-2	102	3.2	2100	62	835	Wedge anchor	12	100	YES	1-s/2-a
Lamanna (2002) [23]	D-1	102	3.2	1117	13.8	232	PAF	4	22	YES	2-a
	D-2			1117	13.8	232		4	22		2-a
	E-1			1117	13.8	232		4	22		2-a
	E-2			1117	13.8	232		4	22		2-a
	J-1			1117	13.8	232		3.7	27		1-a
	L-1			1016	13.8	232		4.5	32		1-a
	T-1			1016	13.8	232		3.7	32		1-a
	T-2			1016	13.8	232		3.7	32		1-a
	T-3			1016	13.8	232		3.7	32		1-a
	F-1			1117	13.8	232		3.7	27		1-a
	G-1			1117	13.8	232		3.7	27		2-a
	K-1			1117	13.8	232		3.7	32		1-a
	M-1			1016	13.8	232		3.7	32		1-a
	N-1			1016	17.0	351		3.7	32		1-a
	P-1		6.4	1016	15.5	204		3.7	27		1-a
	Q-1		3.2	1016	27.3	561		3.7	32		1-a
	R-1			1016	13.8	232		3.5	27		2-a
	R-2			1016	13.8	232		3.5	27		2-a
	U-1	51		1016	13.8	232		3.7	32		1-a
Lamanna *et al.* (2001) [24]	F-42-S-102-1R	102	3.2	1016	13.8	232	PAF	3.5	27	YES	2-a
	F-21-S-102-2R							3.7	32		1-a
Bank *et al.* (2002) Lamanna *et al.* (2004) [25,26]	S-4-Y-AL32	102	3.2	3048	15.2	325	PAF	4.5	32	YES	2-a
	I-4-N-AL32	102			26.3	695			32		2-a
	I-4-Y-AL32	102			26.3	695			32		2-a
	I-4-Y-AL32-R	102			26.3	695			32		2-a
	I-8-Y-AL32	204			26.3	695			32		4-a
	H1.5-4-YAL32	102			57.2	828			32		2-a
	H1.5-4-Y-AL42D	102			57.2	828			42		2-a
	H1.5-4-Y-AL47D	102			57.2	828			47		2-a
	H1.5-4-Y-AL47D-3	102			57.2	828			47		2-a
	H1.5-4-Y-AL47D-3R	102			57.2	828			47		2-a
	H1.5-8-Y-AL32	102			57.2	828			32		4-a
	H1.0-4-Y-AL47D-5	102			56.9	916			47		2-a
Lee *et al.* (2007) [27]	1	102	3.2	1370	68.3	848	PAF	3.5	25	YES	2-a
	2	102	3.2	1370	68.3	848	PAF	3.5	32	YES	2-a
Martin and Lamanna (2008) [28]	6-L	102	3.2	3251	57.7	805	Screw	12.7	50.8	YES	1-a
	6-S										1-s
	10-L										1-a
	12-L										1-a
Napoli *et al.* (2008) [11]	MF-1-L	102	3.2	2718	62	852	Screw	9.5	44.5	NO	1-s
	MF-1-S			2108							1-s
	MF-2-L			2718							1-s
	MF-2-S			2413							1-s

The concretes used for producing members are characterized by medium-high values of the compressive strength, f_c, which can have an influence on the strengthening performance.

The laminates employed for the MF-FRP system have different mechanical properties, determined by mainly varying the combinations of carbon/glass fibers and the amount of embedded fiberglass mats adopted for their manufacturing.

As observed, the mechanical fastening mostly consists of shot fasteners (namely "PAF"), with diameters ranging from 3.5 to 4.5 mm and lengths from 22 to 52 mm.

Screw anchors were also frequently used, for which the diameters span from 4.76 to 12.7 mm and the lengths from 37 to 55 mm. Only in a few cases, instead, the mechanically fastening was performed by using wedge anchors [5,20,22]; in [20,22], they were installed into the concrete by using epoxy resin as a gap filler. In the case of the specimen M-F-P-2 [22], the FRP laminate was both bonded and mechanically fastened to the concrete substrate. In the case of the specimen S-4-F [20], instead, which was pre-cracked prior to being strengthened with the MF-FRP strip, the use of wedge anchors was coupled with end anchor spikes; also, such a member was subjected to a cyclic test unlike the other 92 tests, all monotonic.

4. Application of the FE Model

The FE model has been used for performing numerical simulations of experimental tests collected in the database of Tables 1 and 2. As already mentioned, these analyses were mainly devoted to investigate some specific aspects of the structural response, which may have a varying significance in the modeling of MF-FRP-strengthened beams. In particular, the influence of the following aspects was explored:

(a) uncertainty on the actual mechanical properties of steel rebars and mainly on the f_y value, which is not always provided in the literature papers, and the choice of the stress-strain law to use for simulating the response of such rebars;

(b) selection of the bearing stress-slip interface law to model the effect of the partial interaction between concrete and FRP laminate; and

(c) the cracking process in RC members, related to the different tensile response of concrete, which is generally neglected in modeling methods.

The authors highlight that the numerical analyses have been carried out for all beams listed in Table 1, but, for the sake of brevity, only some of the most representative ones have been chosen in the paper. Furthermore, in order to better show the effect of the three considered parameters on a specific beam, the test, MF-1-L [11] has been selected herein.

4.1. Influence of Mechanical Properties and Stress-Strain Behavior of Steel Rebars

As shown in Table 1, many papers do not provide the actual mechanical properties of the used rebars, as obtained by tensile tests, but only indicate the denomination of the employed steel according to the American Society for Testing and Materials (ASTM) specifications. Thus, some mismatches between experiments and predictions may be related to uncertainties on the steel rebars' properties and mainly on the yield strength value, f_y.

Figure 8a,b depicts the numerical simulations obtained for three tests, namely P-1 [23], -1 and -2 [27]. For these analyses, the behavior of the steel rebars was modeled according to the stress-strain

relationship of Figure 5a and by plugging two alternative values of the yield strength, *i.e.*, f_y = 420 MPa, which is the lowest strength attributable to Grade 60 steel and a slightly increased value equal to 475 MPa; then, an ultimate strength $f_t = 1.2 \cdot f_y$ was always considered. In these tests, the concrete-FRP interface was modeled through the σ_f-s law proposed by Elsayed *et al.* [17], *i.e.*, Model 1 of Figure 6 which is the only one available for the case of shot fasteners; the tension stiffening effect was taken into account by considering C = 1 in Equation (6).

Figure 8. Influence of the mechanical properties (**a**,**b**,**e**) and stress-strain law (**c**,**d**,**f**) of steel rebars.

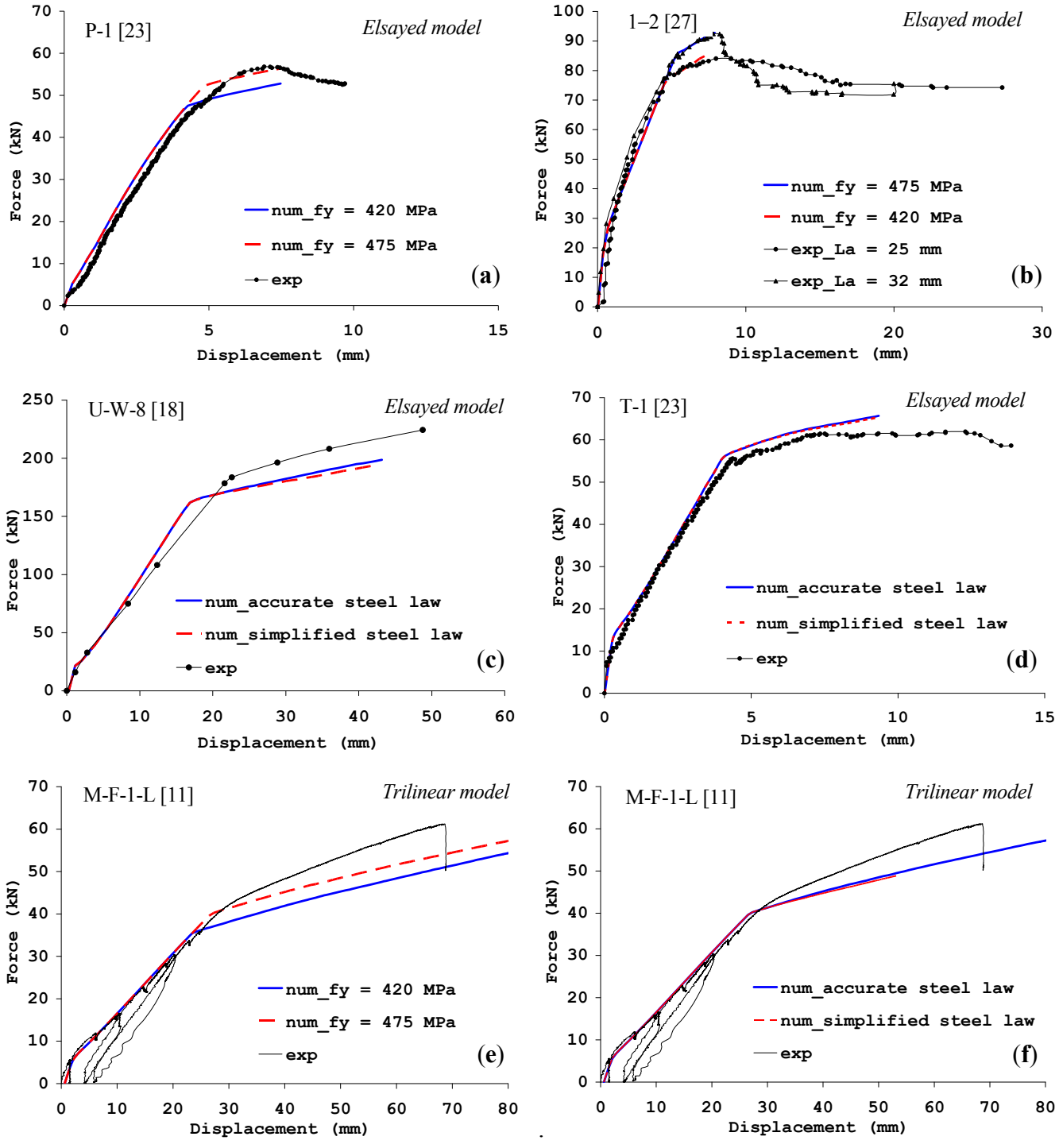

The comparisons of Figure 8a,b highlight the good accuracy of the performed modeling, thus implying that uncertainties on the steel rebars' properties are well covered by the range chosen for f_y. In fact, for the test, P-1, the numerical simulation obtained by considering f_y = 420 MPa reproduces the experimental curve well in terms of initial stiffness but underestimates the flexural response at the peak condition; conversely, the numerical curve resulting from f_y = 475 MPa approximates the post-yield behavior better. By looking at the plot of Figure 8b, instead, it is noted that each numerical simulation accurately reproduces one of the two experimental curves; such curves differ from each other for the length of the used fastener (L_a = 25 or 32 mm).

A further aspect of interest in the modeling of the steel rebars' behavior deals with the approximation level achieved when the elastic plastic stress-strain law (Figure 5b) is used in place of the more accurate one shown in Figure 5a. To this aim, the experimental-numerical comparisons shown in Figure 8c,d can be observed, which were obtained for specimens U-W-8 [18] and T-1 [23]. As for the tests P-1, -1 and -2, the behavior of the FRP–concrete interface was modeled through the σ_f-s law proposed by Elsayed *et al.* [17] for the case of "PAF" systems. As expected, Figure 8c,d confirms a rather slight dependence of the numerical curves on the model type used for steel rebars; therefore, the elastic-plastic law can be successfully chosen for the simulations of all tests.

The low influence of mechanical properties and the stress-strain behavior of steel rebars can be finally verified by observing the experimental-numerical comparisons in Figure 8e,f, obtained for specimen MF-1-L [11]. In this test, the behavior of the FRP-concrete interface was modeled through the σ_f-s law proposed by Realfonzo *et al.* [16] and suitable for fasteners w/o washers (*i.e.*, Model 3 in Figure 6); the tension stiffening effect was taken into account by considering C = 1 in Equation (6). As shown, the post-yield behavior of the experimental curve is better simulated by considering f_y = 475 MPa in the numerical analysis, whereas no appreciable influence is noted by changing the stress-strain model for steel rebars.

4.2. Influence of the Bearing Stress–Slip Interface Law

As mentioned earlier, Elsayed *et al.* [17] and Realfonzo *et al.* [16] recently proposed nonlinear bearing stress–slip models to describe the effect of the partial interaction between the concrete and the FRP laminate. These models, depicted in Figure 6, were experimentally calibrated through direct shear (DS) tests performed on MF-FRP/concrete joints with a single connector.

In particular, among the proposals by Elsayed *et al.*, one model was found from joints having a shot fastener with a 47-mm shank length, a 3.7-mm shank diameter and a 13-mm washer; the other one, instead, was defined for a screwed fastener with a 37-mm shank length, a 4.8-mm shank diameter and a 16-mm washer.

The trilinear models proposed by Realfonzo *et al.* were found from a screwed fastener w/ or w/o washer; the screw adopted in the DS tests had a 45-mm shank length, a 6-mm shank diameter and a 32-mm washer (when used).

Comparisons between experimental and numerical force-deflection curves are shown in Figure 9, which allow one to better investigate the sensitivity of the structural response with the use of different bearing stress–slip relationships. It is highlighted that in these tests, the tension stiffening effect was taken into account by considering C = 1 in Equation (6).

Figure 9. Influence of the bearing stress-slip interface law: numerical simulations of tests by Ebead [19] (**a**–**d**) and Napoli *et al*. [11] (**e**–**h**).

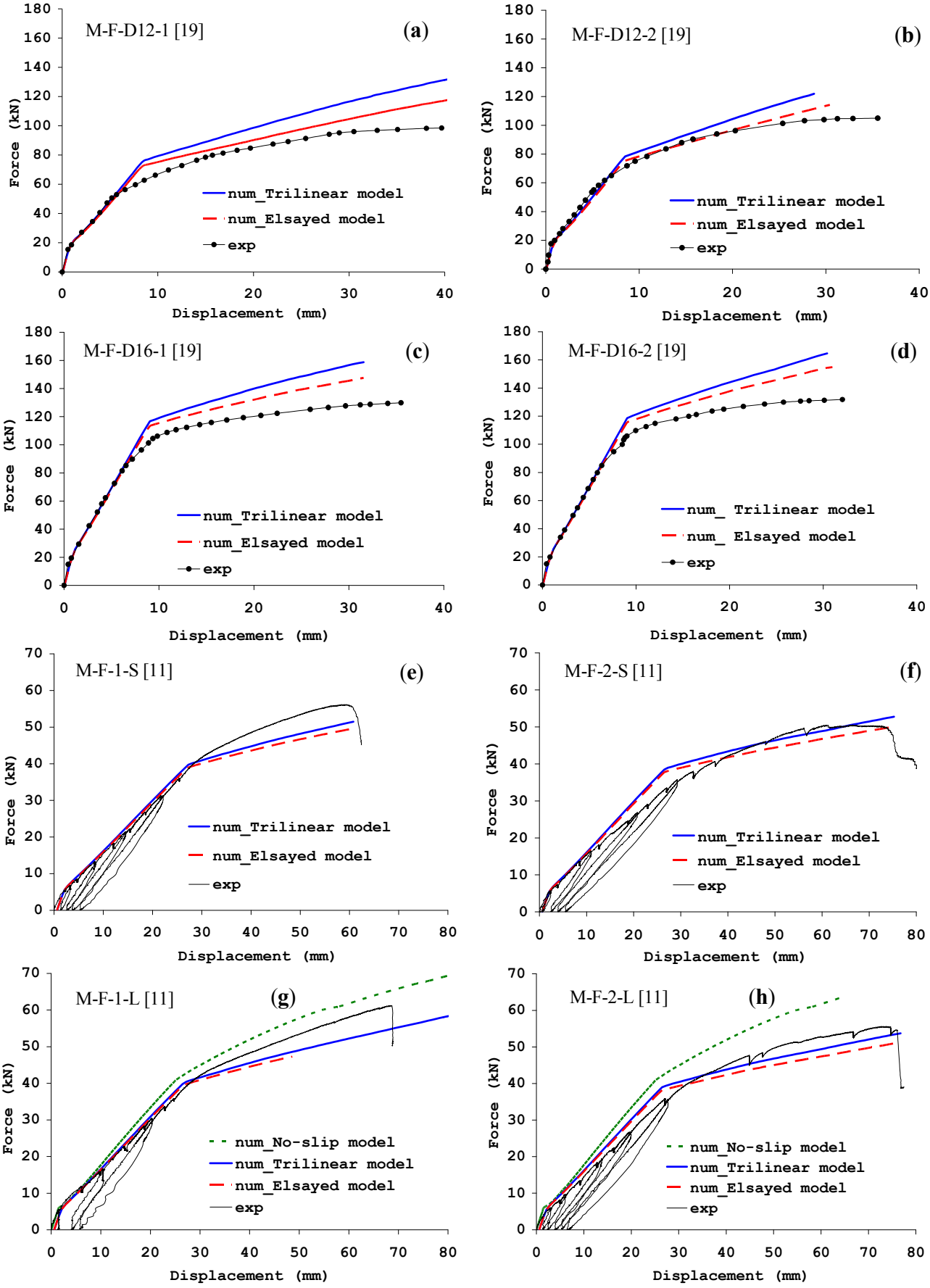

In the plots of Figure 9a–d, obtained for some tests performed by Ebead [19], the behavior of the screws w/ washer was modeled by using the respective σ_f-s laws provided by Elsayed *et al.* ("Elsayed model") and Realfonzo *et al.* ("Trilinear model"), *i.e.*, Models 2a and 2b in Figure 6. As observed, both simulations well reproduce the initial stiffness of the experimental curves, since the two bearing stress-slip models overlap each other for low values of interfacial slips (Figure 6). Then, increasing the relative displacement between the concrete and FRP strip, a greater force per fastener is calculated with the trilinear σ_f-s law which in turn leads to overestimating of the flexural strength of the beams. Thus, although differences between the two simulations are rather negligible, the numerical predictions obtained by assuming the "Elsayed model" better predict the three experimental curves; this evidence may be partially justified by the fastener type used in the tests by Ebead [19], which is the same employed by Elsayed *et al.* [17] in the DS tests.

In Figure 9e–h, the behavior of screws w/o washer in tests by Napoli *et al.* [11] was modeled by using Model 3 in Figure 6 by Realfonzo *et al.* [16] and, for comparison, Model 1 by Elsayed *et al.* [17], though suitable for fasteners w/ washer. Furthermore, in order to better highlight how the use of a proper bearing stress-slip law improves the fitting of the experimental results, in Figure 9g,h the results of numerical simulations obtained by implementing a "no-slip" model of the MF-FRP connection are reported.

In the case of tests MF-1-S and MF-1-L, the plots show a very good agreement between experimental results and numerical predictions, which are rather accurate in simulating the cracking onset in concrete and yielding in steel rebars. In the cases of tests MF-2-L and MF-2-S, the numerical responses before steel yielding are characterized by a slightly greater stiffness with respect to the experimental ones. In all cases, since small values of interfacial slips are activated for these members, the numerical simulations do not significantly change with the use of the two σ_f-s relationships, thus implying that both of them are suitable for modeling MF-FRP-strengthened slabs.

4.3. Influence of the Tension-Stiffening Effect

The simulation of the cracking processes of RC members is a challenging issue, especially in the case of 1D numerical models. Such processes are characterized by the onset of cracking in concrete subjected to tensile stresses: since the actual tensile strength of concrete is generally affected by significant levels of randomness, the prediction of the cracking onset is often a critical issue. Furthermore, the well-known tension-stiffening effect significantly influences the flexural response of RC members in the post-cracking stage.

As mentioned earlier, since the present proposal is based on a continuous (smeared) crack FE model, the tension stiffening effect has been simulated by a conventional softening branch in the tensile stress-strain law of concrete, which is expressed by the following equation [15]:

$$\sigma_c = f_{ct} \cdot \left(\frac{f_{ct}/E_{ct}}{|\varepsilon|} \right)^C \text{ with } \varepsilon < f_{ct}/E_{ct} \tag{6}$$

where f_{ct} is the nominal tensile strength, E_{ct} the Young modulus of concrete in tension and C a conventional exponent controlling the post-peak softening branch of concrete.

It is worth highlighting that the shape of the post-peak tensile branch strongly depends on the values of the *C* exponent in Equation (6). Since this exponent is intended at a "material level" simulation of the tension-stiffening effect (which is rather a structural effect), no constitutive correlation can be figured out for *C*, but its value should be calibrated depending on the geometric and mechanical properties of the RC member under consideration. In this study, the tension stiffening effect is investigated by considering three fairly different values of such a *C* exponent, spanning over a range from 0.5 to 50 and covering tensile behaviors of concrete from rather resilient ($C = 0.5$) to very brittle ($C = 50$).

Figure 10 shows the resulting numerical simulations for some tests reported in [11,18,23,25,26]. It is highlighted that the behavior of fasteners has been simulated by using: Model 1 by Elsayed *et al.* [17] for tests U-W-6 and T-1; the trilinear σ_f-s Models 2b and 3 by Realfonzo *et al.* [16] for test M-F-1-L and I-4-N-AL32, respectively.

Figure 10. Influence of the tension-stiffening effect: numerical simulations of tests by Borowicz [18] (**a**); Lamanna [23] (**b**); Napoli *et al.* [11] (**c**); Bank *et al.* and Lamanna *et al.* [25,26] (**d**).

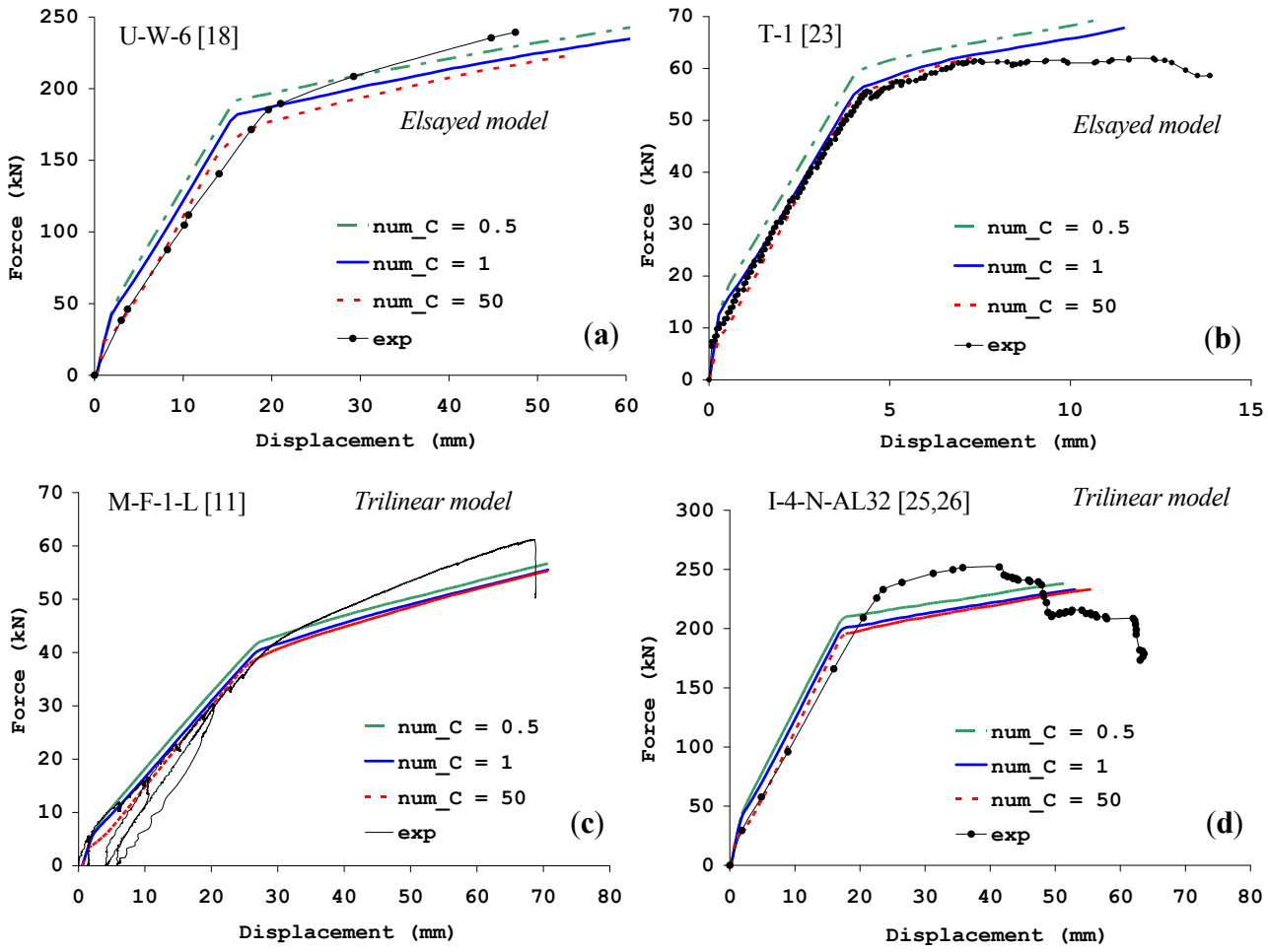

Observing these plots, it is noted that the effect of a different tensile response of concrete is particularly relevant in terms of flexural stiffness in the post-cracking regime. However, a lower tension-stiffness effect (simulated by assuming $C = 50$) has an influence on the bending moment of the beam at yielding. Particularly, it results in the most accurate simulations in terms of initial stiffness

when shot fasteners are used (see Figure 10a,b,d). In fact, the installation of such a connector type generally induces significant pre-cracking in the concrete, which is well reproduced by a lower contribution of the tension-stiffening effect.

5. Conclusions

A finite element model was developed and used by the authors to simulate the flexural behavior of RC beams externally strengthened by mechanically fastened FRP laminates.

Several numerical analyses were carried out by using experimental results collected in a wide database assembled from the literature. Such analyses were aimed at investigating the influence of some specific aspects on the structural response of MF-FRP strengthened members, such as stress-strain laws implemented for steel rebars, bearing stress-slip laws assumed for the FRP-concrete interface and the cracking process, with emphasis on the tension stiffening effect developing in RC members.

From the experimental-numerical comparisons, the following considerations were drawn and can be generalized in the modelling of MF-FRP-strengthened members:

(a) as expected, a rather slight dependence of the performed analyses on the stress-strain model used for steel rebars is observed; thus, a simplified elastic-plastic law can be successfully chosen in the simulation of tests;

(b) since small values of interfacial slips are activated in the case of MF-FRP-strengthened beams, the numerical simulations do not significantly change with the use of two different bearing stress-slip relationships, thus implying that both of them are suitable in the modeling of these members;

(c) the use of a lower tension-stiffening effect has an influence on the bending moment of the beam at yielding and provides the most accurate simulations in terms of initial stiffness when shot fasteners are used. In fact, the installation of such a connector type generally induces significant pre-cracking in the concrete, which is well reproduced by a lower contribution of the tension-stiffening effect. For the case of fastening with concrete screws or wedge anchors, instead, the implementation of the tension-stiffening effect with the C exponent equal to one generally provides the most accurate simulation of the experimental results.

Conflicts of Interest

The authors declare no conflict of interest.

References

1. Strongwell, 2010. Available online: http://www.strongwell.com (accessed on 27 January 14).
2. Bank, L.C. Mechanically-Fastened FRP (MF-FRP)—A Viable Alternative for Strengthening RC Members. In Proceedings of the FRP Composites in Civil Engineering (CICE 2004), Adelaide, Australia, 8–10 December 2004.
3. Rizzo, A.; Galati, N.; Nanni, A.; Bank, L.C. Strengthening Concrete Structures with Mechanically Fastened Pultruded Strips. In Proceedings of the Composites 2005, Columbus, OH, USA, 28–30 September 2005.

4. Brown, V.L.; Bank, L.C.; Arora, D.; Borowicz, D.T.; Godat, A.; Lamanna, A.J.; Lee, J.; Matta, F.; Napoli, A.; Tan, K.H. Experimental studies of mechanically-fastened FRP systems: State-of-the-art. In *ACI Special Publication SP-275-48,* Proceedings of the FRPRCS-10, Tampa Bay, FL, USA, 2–4 April 2011; pp. 841–886.
5. El-Maaddawy, T. Mechanically fastened composites for retrofitting corrosion-damaged reinforced-concrete beams: Experimental investigation. *J. Compos. Constr.* **2013**, doi:10.1061/(ASCE)CC.1943-5614.0000447.
6. Dempsey, D.D.; Scott D.W. Wood members strengthened with mechanically fastened FRP strips. *J. Compos. Constr.* **2006**, *10*, 392–398.
7. Schorer, A.E.; Bank, L.C.; Oliva, M.G.; Wacker, J.P.; Rammer, D.C. Feasibility of Rehabilitating Timber Bridges Using Mechanically Fastened FRP Strips. In Proceedings of the ASCE SEI Structures 2008 Conference, Crossing Borders, Vancouver, BC, Canada, 24–26 April 2008.
8. Napoli, A.; Bank, L.C.; Brown, V.L.; Martinelli, E.; Matta, F.; Realfonzo, R. Analysis and design of RC structures strengthened with mechanically fastened FRP laminates: A review. *Compos. B Eng.* **2013**, *55*, 386–399.
9. Lee, J.H.; Lopez, M.M.; Bakis, C.E. Slip effects in reinforced concrete beams with mechanically fastened FRP strip. *Cem. Concr. Compos.* **2009**, *31*, 496–504.
10. Nardone, F.; Lignola, G.P.; Prota, A.; Manfredi, G.; Nanni, A. Modeling of flexural behavior of RC beams strengthened with mechanically fastened FRP strips. *Compos. Struct.* **2011**, *93*, 1973–1985.
11. Napoli, A.; Matta, F.; Martinelli, E.; Nanni, A.; Realfonzo, R. Modelling and verification of response of RC slabs strengthened in flexure with mechanically fastened FRP laminates. *Mag. Concr. Res.* **2010**, *62*, 593–605.
12. Martinelli, E.; Napoli, A.; Nunziata, B.; Realfonzo, R. A 1D finite element model for the flexural behaviour of RC beams strengthened with MF-FRP strips. *Compos. Struct.* **2014**, *107*, 190–204.
13. Faella, C.; Martinelli, E.; Nigro, E. Formulation and validation of a theoretical model for intermediate debonding in FRP strengthened RC beams. *Compos. B Eng.* **2008**, *39*, 645–655.
14. Popovics, S. A numerical approach to the complete stress strain curve for concrete. *Cem. Concr. Res.* **1973**, *3*, 583–559.
15. Okamura, H.; Maekawa, K.; Sivasubramaniyam, S. Verification of Modeling for Reinforced Concrete Finite Element. In *Finite Element Analysis of Reinforced Concrete Structures*, Proceedings of the Seminar ASCE, Tokyo, Japan, 21–24 May 1985; pp. 528–543.
16. Realfonzo, R.; Martinelli, E.; Napoli, A.; Nunziata, B. Experimental investigation of the mechanical connection between FRP laminates and concrete. *Compos. B: Eng.* **2013**, *45*, 341–355.
17. Elsayed, W.E.; Ebead, U.A.; Neale, K.W. Studies on mechanically fastened fiber-reinforced polymer strengthening systems. *ACI Struct. J.* **2009**, *106*, 49–59.
18. Borowicz, D.T. Rapid Strengthening of Concrete Beams with Powder-Actuated Fastening Systems and Fiber Reinforced Polymer (FRP) Composite Materials. MSc Thesis, University of Wisconsin-Madison, Madison, WI, USA, 2002.
19. Ebead, U. Hybrid externally bonded/mechanically fastened fiber-reinforced polymer for RC beam strengthening. *ACI Struct. J.* **2011**, *108*, 669–678.

20. Ekenel, M.; Rizzo, A.; Myers, J.J.; Nanni, A. Flexural fatigue behavior of reiforced concrete beams strengthened with FRP fabric and precured laminate systems. *J. Comp. Constr.* **2006**, *10*, 433–442.
21. El-Maaddawy, T.; Nessabi, A.; El-Dieb, A. Flexural response of corroded reinforced concrete beams strengthened with powder-actuated fastened composites. *J. Compos. Constr.* **2013**, doi:10.1061/(ASCE)CC.1943-5614.0000395.
22. Galati, D.; Rizzo, A.; Micelli, F. Comparison of reinforced concrete beams strengthened with FRP pre-cured laminate systems and tested under flexural loading. In Proceedings of the FRPRCS-8, Patras, Greece, 16–18 July 2007.
23. Lamanna, A.J. Flexural Strengthening of Reinforced Concrete Beams with Mechanically Fastened Fiber Reinforced Polymer Strips. Ph.D. Thesis, University of Wisconsin-Madison, Madison, WI, USA, 2002.
24. Lamanna, A.J.; Bank, L.C.; Scott, D.W. Flexural strengthening of reinforced concrete beams using fasteners and fiber-reinforced polymer strips. *ACI Struct. J.* **2001**, *98*, 368–376.
25. Bank, L.C.; Lamanna, A.J.; Ray, J.C.; Velazquez, G.I. *Rapid Strengthening of Reinforced Concrete Beams with Mechanically Fastened, Fiber Reinforced Polymeric Composites Materials*, Report ERDC/GSL TR-02-4; US Army Corps of Engineers: Madison, WI, USA, 2002; pp. 1–99.
26. Lamanna, A.J.; Bank, L.C.; Scott, D.W. Flexural strengthening of reinforced concrete beams by mechanically attaching fiber-reinforced polymer strips. *J. Compos. Constr.* **2004**, *8*, 203–210.
27. Lee, H.L.; Lopez, M.M.; Bakis, C.E. Flexural behavior of reinforced concrete beams strengthened with mechanically fastened FRP strip. In Proceedings of the FRPRCS-8, Patras, Greece, 16–18 July 2007.
28. Martin, J.A.; Lamanna, A.J. Performance of mechanically fastened FRP strengthened concrete beams in flexure. *J. Compos. Constr.* **2008**, *12*, 257–265.